Nonlinear electromechanical coupling in graded soft materials:
Large deformation, instability, and electroactuation

Lingling Chen [1] Xu Yang,[1] Binglei Wang,[1,*] and Shengyou Yang [1,2,†]

[1]*Department of Engineering Mechanics, School of Civil Engineering, Shandong University, Jinan 250061, China*
[2]*Suzhou Research Institute, Shandong University, Jiangsu 215123, China*

Subject to an applied electric field, soft dielectrics with intrinsic low moduli can easily achieve a large deformation through the so-called electrostatic Maxwell stress. Meanwhile, the highly nonlinear electromechanical coupling between the mechanical and electric loads in soft dielectrics gives a variety of failure modes, especially pull-in instability. These failure modes make the application of soft dielectrics highly limited. In this paper, we investigate the large deformation, pull-in instability, and electroactuation of a graded circular dielectric plate subject to the in-plane mechanical load and the applied electric load in the thickness direction. The results obtained herein cover, as special cases, the electromechanical behaviors of homogeneous dielectrics. There is a universal physical intuition that stiffer dielectrics can sustain higher electromechanical loads for pull-in instability but achieve less deformation, and vice versa. We show this physical intuition theoretically in different homogeneous dielectrics and graded dielectrics. Interestingly, we find that the ability to sustain a high electric field or a large deformation in a stiff or soft homogeneous circular dielectric plate can be achieved by just using a graded circular dielectric plate. We only have to partly change the modulus of a circular plate, with a stiff or soft outer region. The change makes the same electromechanical behavior as that of a homogeneous dielectric, even increases the maximum electroactuation stretch from 1.26 to 1.5. This sheds light on the effects of the material inhomogeneity on the design of advanced dielectric devices including actuators and energy harvestors.

I. INTRODUCTION

Soft dielectrics have intrinsically low elastic stiffness and can be easily deformed to achieve significantly large deformations by applying an external electric field. The mechanism for the large deformation can be attributed to the highly nonlinear electromechanical coupling between mechanical and electric fields. By harnessing the electrically activated large deformation and the rich variety of electromechanical behaviors, soft dielectrics have been investigated for numerous tantalizing applications in soft actuators [1–5], humanlike robots [6,7], stretchable electronics [8,9], energy harvesters [10–15], among others.

Large deformations in soft dielectrics invariably lead to the possibility of electromechanical failure. Some standard modes of failure are briefly listed here, for example, the electromechanical instability [16–32], rupture by stretch [17,33], and electric breakdown [1,16,17,34,35]. Moreover, the electromechanical instability can be simply classified into a number of types: pull-in instability [16–19,21–24], electrobuckling [25–27], electrowrinkling [28–30], and electrocreasing [30,31], bursting drops in solid dielectrics [32], among others. Electromechanical instabilities are often thought to be detrimental to the functionality of the device composed of dielectric electroactive polymers (EAPs); therefore, a number of approaches have been used to suppress or avoid the electromechanical instabilities in soft dielectric devices. On the other hand, instabilities can be harnessed for numerous applications such as producing true musclelike actuation [36], generating hierarchical topographical patterns [37], achieving giant voltage-triggered deformation via snap-through [38,39], among others [40–42].

In this paper, we focus on large deformation, pull-in instability, and electroactuation of a circular plate of dielectric elastomers. Consider a simple but classic dielectric elastomer actuator [1,2,23] that is made of a dielectric thin film sandwiched between two compliant electrodes. Upon application of a voltage difference between the top and bottom electrodes, the dielectric film thins down in thickness and expands in area due to the so-called Maxwell stress. When the applied voltage increases up to the threshold, the dielectric film cannot sustain the electric load any more and then pull-in instability occurs.

To make a better understanding of the large deformation of a dielectric film actuator, we plot a schematic (see Fig. 1) to show how the circular dielectric plate deforms under the combination of the electromechanical loads. Detailed descriptions can be found in the caption. Theoretical results [18,41] show that in the absence of the prestress the maximum actuation stretch is 1.26. The functionality of a dielectric actuator is highly restricted by the maximum actuation stretch and the critical nominal electric field. Therefore, elaborate efforts have been made to suppress or avoid the onset of pull-in instability, and then increase the maximum electroactuation

---

*Corresponding author: bwang@sdu.edu.cn
†Corresponding author: syang_mechanics@sdu.edu.cn
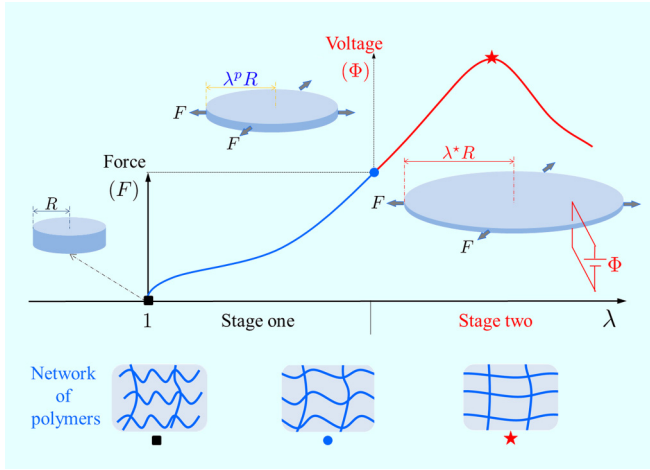
FIG. 1. Schematic of the large deformation and pull-in instability of dielectric elastomers subjected to electromechanical loads. An undeformed circular dielectric plate with radius R is marked by a square (■) on the horizontal axis at $\lambda = 1$. In stage one, the circular plate is only subjected to a purely mechanical load and the radius continuously increases to $\lambda^p R$ as the force increases to F, which is marked by a circle (●). In stage two, we keep the magnitude of the force F and begin to increase the applied voltage Φ in the thickness direction. As the applied voltage increases to the threshold [marked by a star (★) on the curve], the circular dielectric plate expands its radius to $\lambda^\star R$ and cannot sustain the applied voltage any more. At this moment, pull-in instability occurs and then the circular plate thins its thickness quickly and expands its in-plane area dramatically until the occurrence of electric breakdown. The schematic of the molecular chains at three different states are also plotted.

and the critical nominal electric field. For instance, either a pre-stretch [15,18,24,43] or a material with load-dependent stiffening [44,45] can be used to suppress or delay pull-in instability and then increase the actuation strain.

Motivated by the theoretical thresholds of the maximum actuation stretch and the critical nominal electric field of a homogeneous dielectric film in the work [18,41], we investigate the effects of material heterogeneity on the large deformation, pull-in instability, and electroactuation of an inhomogeneous dielectric film. To avoid a complicated mathematical presentation and highlight the physical implications behind the material heterogeneity, we consider an inhomogeneous circular dielectric plate whose modulus varies along the radial direction in our theoretical model. The idea of a graded modulus can also be found in the analysis of surface instability of compressed soft materials [46]. In this paper, we would like to seek how the varied modulus affects the nonlinear electromechanical coupling, and under which condition pull-in instability can be delayed and the circular dielectric plate can achieve a relatively large electroactuation strain.

This paper is organized as follows. Section II is about the basic formulation of the electromechanical coupling of a graded circular dielectric plate subjected to an in-plane traction force and an applied voltage in the thickness direction. In Sec. III, we carry out our analysis by considering a graded neo-Hookean solid. We solve the boundary-value problem analytically and then use the linear bifurcation analysis to derive the condition for the onset of pull-in instability. Results
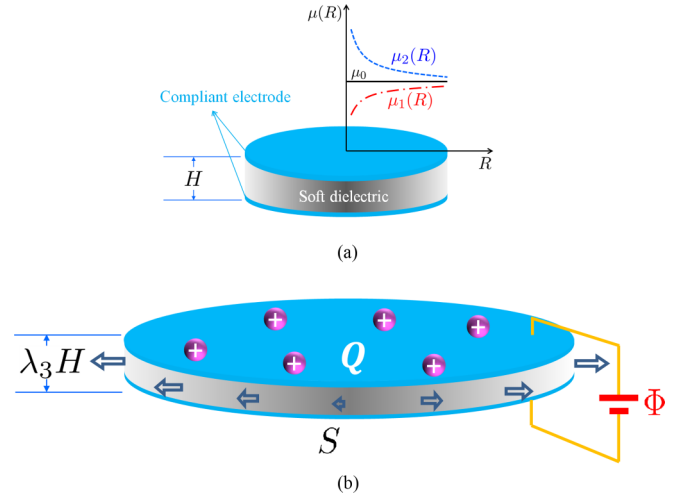
FIG. 2. Schematic of the deformation of a circular dielectric plate subjected to an electric voltage Φ in the thickness direction and a dead load S in the radial direction. The modulus of the dielectric elastomer can vary with the radius, i.e., the shear modulus $\mu(R)$ is a function of the radius R. The circular plate is coated with two compliant electrodes on the top and bottom surfaces. (a) Undeformed circular plate with radius B and thickness H. (b) Deformed circular plate with thickness $h = \lambda_3 H$ and each electrode gains an electric charge of magnitude Q.

and discussions are given in Sec. IV. Concluding remarks and possible future research are given in Sec. V.

II. FORMULATION

Consider a circular dielectric plate with radius B and thickness H in the undeformed state (see Fig. 2). Taking the cylindrical coordinates (R, Θ, Z) with an *orthonormal* basis (e_R, e_Θ, e_Z), the domain of the circular dielectric plate in the reference configuration is represented by

$$\Omega_R = \{(R, \Theta, Z) \in \mathbb{R}^3 : 0 \leqslant R \leqslant B,$$
$$0 \leqslant \Theta < 2\pi, \; 0 \leqslant Z \leqslant H\}. \quad (1)$$

The mechanical boundary condition on the lateral surface is

$$\boldsymbol{T} e_R = S e_R \quad \text{at } R = B, \quad (2)$$

where $\boldsymbol{T}$ is the total nominal stress and S is the traction force on the lateral surface. On the top and bottom surfaces, the mechanical boundary conditions are

$$\boldsymbol{T} e_Z = \boldsymbol{0} \quad \text{at } Z = 0, \, H, \quad (3)$$

while the electric boundary conditions are

$$\xi = 0 \quad \text{at } Z = 0 \quad \text{and} \quad \xi = \Phi \quad \text{at } Z = H, \quad (4)$$

where ξ is the electric potential and Φ is an applied voltage. The nominal electric field is defined as

$$\tilde{\boldsymbol{E}} = \frac{\Phi}{H} e_Z = \tilde{E} e_Z. \quad (5)$$

Note that $\tilde{\boldsymbol{E}}$ in (5) comes from the Maxwell equations $\tilde{\boldsymbol{E}} = -\nabla \xi$ and $\nabla \cdot \tilde{\boldsymbol{D}} = 0$, the relation between $\tilde{\boldsymbol{E}}$ and $\tilde{\boldsymbol{D}}$, as well as

the electric boundary conditions (4). Here we omit the tedious mathematical calculations for simplicity.

A. Large deformation

Subject to the nominal electric field $\tilde{E}$ in the thickness direction (the Z direction) and a uniform traction force S in the radial direction[1], the circular dielectric plate expands its in-plane area and decreases its thickness from H to $h = \lambda_3 H$. Here the stretch λ_3 is assumed to be a *constant* that is independent of the position. Therefore, only the homogeneous thinning phenomena of electromechanical couplings are addressed in this paper. Generally, the deformed thickness of the dielectric elastomer can vary with the coordinates, which makes the inhomogeneous thinning possible, for example, the electrocreasing instabilities in soft electroactive elastomers [31].

In addition to the homogeneous thinning, i.e., a constant stretch λ_3, we consider the cylindrical deformation in which the deformation x has the following component form:

$$r = r(R), \quad \theta = \Theta, \quad z = \lambda_3 Z. \qquad (6)$$

We remark that the cylindrical deformation is just one of the admissible deformations. Other deformations may also exist during the homogeneous thinning of the dielectric elastomer, but they are out of the scope of this paper.

By the cylindrical deformation (6), the deformation gradient F in the cylindrical coordinates has the following component form, which is represented by a diagonal matrix,

$$F := \mathrm{diag}\left(r', \frac{r}{R}, \lambda_3\right). \qquad (7)$$

Here and henceforth, the prime denotes the partial derivative with respect to R. For simplicity, we take the following notations:

$$x = x(R) = r' \quad \text{and} \quad y = y(R) = \frac{r}{R}. \qquad (8)$$

Incompressibility requires that the Jacobian J must be one, i.e.,

$$J = \det F = r'\frac{r}{R}\lambda_3 = xy\lambda_3 = 1. \qquad (9)$$

B. Mechanical and electric stresses

The total nominal stress T is denoted by

$$T = \frac{\partial W^e}{\partial F} + T^M - \kappa F^{-T}. \qquad (10)$$

Here W^e is the strain-energy function of the purely elastic part, T^M is the nominal Maxwell stress, κ serves as the Lagrange multiplier, and F^{-T} is the inverse of the transpose F^T. For a linear dielectric (see, for example, [41,47]), the dielectric constant ε is constant[2] and the nominal Maxwell

---

[1]The resultant force on the outer surface is equal to $S\,2\pi BH$. We remark that the nominal electric field $\tilde{E}$ and the dead load S are constant during the thinning of the circular dielectric plate.

[2]The dielectric constant can vary with the strain, which is known as electrostriction; see, for example, [49,50]. The varied dielectric constant is not considered in this paper.

stress T^M can be expressed as

$$T^M = \frac{1}{\varepsilon J}(F\tilde{D}) \otimes \tilde{D} - \frac{1}{2\varepsilon J}|F\tilde{D}|^2 F^{-T}, \qquad (11)$$

where "$\otimes$" denotes the tensor product and $\tilde{D}$ is the nominal electric displacement. The relation between $\tilde{D}$ and the nominal electric field $\tilde{E}$ for a linear dielectric is

$$\tilde{D} = \varepsilon J C^{-1}\tilde{E}, \qquad (12)$$

where C^{-1} is the inverse of the right Cauchy-Green tensor $C = F^T F$.

Since the deformation gradient F is represented by a diagonal matrix in (7), the right Cauchy-Green tensor is $C := \mathrm{diag}\,(x^2, y^2, \lambda_3^2)$ and its inverse is $C^{-1} := \mathrm{diag}\,(x^{-2}, y^{-2}, \lambda_3^{-2})$. By (5), the nominal electric displacement in (12) is

$$\tilde{D} = \varepsilon\tilde{E}\lambda_3^{-2}e_Z, \qquad (13)$$

and then the nominal Maxwell stress in (11) is

$$T^M := \frac{\varepsilon\tilde{E}^2\lambda_3^{-2}}{2}\mathrm{diag}\left(-x^{-1}, -y^{-1}, \lambda_3^{-1}\right). \qquad (14)$$

Assuming isotropy, the strain-energy function $W^e(F)$ depends on the deformation gradient F through the principal stretches x, y, and λ_3 in (7), i.e., $W^e(F) = W^e(x, y, \lambda_3)$. Then the elastic stress tensor can be expressed as

$$\frac{\partial W^e}{\partial F} - \kappa(R)F^{-T} := \mathrm{diag}\left(\frac{\partial W^e}{\partial x} - \kappa(R)x^{-1}, \frac{\partial W^e}{\partial y} - \kappa(R)y^{-1},\right.$$
$$\left.\frac{\partial W^e}{\partial\lambda_3} - \kappa(R)\lambda_3^{-1}\right). \qquad (15)$$

It follows from (14) and (15) that the total nominal stress T in (10) is

$$T := \mathrm{diag}\,(T_1, T_2, T_3), \qquad (16)$$

where the principal stresses are

$$T_1 = \frac{\partial W^e}{\partial x} - \left(\kappa(R) + \frac{\varepsilon\tilde{E}^2\lambda_3^{-2}}{2}\right)x^{-1},$$
$$T_2 = \frac{\partial W^e}{\partial y} - \left(\kappa(R) + \frac{\varepsilon\tilde{E}^2\lambda_3^{-2}}{2}\right)y^{-1},$$
$$T_3 = \frac{\partial W^e}{\partial\lambda_3} - \left(\kappa(R) - \frac{\varepsilon\tilde{E}^2\lambda_3^{-2}}{2}\right)\lambda_3^{-1}. \qquad (17)$$

C. Equilibrium equation and boundary conditions

Without the body force, the equilibrium equation reads Div $T = 0$. By (16) and the divergence in cylindrical coordinates, we obtain the only nontrivial equation,

$$\frac{\partial T_1}{\partial R} + \frac{T_1 - T_2}{R} = 0. \qquad (18)$$

By (16), the boundary conditions (2) read

$$T_1 = S \quad \text{at } R = B, \qquad (19)$$

and the boundary conditions (3) are

$$T_3 = 0 \quad \text{at } Z = 0,\ H. \qquad (20)$$

Note that T_1, T_2, and T_3 in (18) are defined by (17). Here we would like to further simplify expression of the equilibrium equation. Consider the following term,

$$\frac{d}{dR}(x^{-1}) + \frac{1}{R}(x^{-1} - y^{-1}) = -x^{-2}\frac{dx}{dR} + \frac{1}{R}(x^{-1} - y^{-1}). \tag{21}$$

By (8), we have the derivative $y' = \frac{1}{R}(r' - \frac{r}{R}) = \frac{1}{R}(x - y)$. In addition, taking the partial derivative of the constraint (9) with respect to R, we have $x'y + xy' = 0$. Thus, we obtain $x' = -xy'/y = -\frac{x(x-y)}{Ry}$ and $-x^{-2}x' = \frac{(x-y)}{Rxy} = \frac{1}{R}(y^{-1} - x^{-1})$. Hence, the term (21) is equal to zero and the equilibrium equation (18) is then written as

$$\frac{\partial}{\partial R}\left(\frac{\partial W^e}{\partial x} - \kappa x^{-1}\right)$$
$$+ \frac{1}{R}\left(\frac{\partial W^e}{\partial x} - \frac{\partial W^e}{\partial y} - \kappa(x^{-1} - y^{-1})\right) = 0. \tag{22}$$

By the chain rule, we have $\frac{\partial}{\partial R} = \frac{\partial y}{\partial R}\frac{\partial}{\partial y} = \frac{1}{R}(x - y)\frac{\partial}{\partial y}$, where the derivative $\frac{\partial y}{\partial R} = \frac{1}{R}(x - y)$ is used. Therefore, the equilibrium equation (22) can be further recast as

$$(x - y)\frac{\partial}{\partial y}\left(\frac{\partial W^e}{\partial x} - \kappa x^{-1}\right)$$
$$+ \left(\frac{\partial W^e}{\partial x} - \frac{\partial W^e}{\partial y} - \kappa(x^{-1} - y^{-1})\right) = 0. \tag{23}$$

D. Summary of the boundary-value problem

Based on the analysis in Secs. II A–II C, we summarize the boundary-value problem (BVP) of the nonlinear electromechanical coupling of a deformable graded circular plate in the reference configuration as follows:

Kinematics :

$$x = r', \ y = \frac{r}{R}, \ xy\lambda_3 = 1,$$

Equilibrium equation :

$$(x - y)\frac{\partial}{\partial y}\left(\frac{\partial W^e}{\partial x} - \kappa x^{-1}\right)$$
$$+ \left(\frac{\partial W^e}{\partial x} - \frac{\partial W^e}{\partial y} - \kappa(x^{-1} - y^{-1})\right) = 0,$$

Mechanical BCs :

$$\frac{\partial W^e}{\partial x} - \left(\kappa(R) + \frac{\varepsilon\tilde{E}^2\lambda_3^{-2}}{2}\right)x^{-1} = S \text{ at } R = B,$$

$$\frac{\partial W^e}{\partial \lambda_3} - \left(\kappa(R) - \frac{\varepsilon\tilde{E}^2\lambda_3^{-2}}{2}\right)\lambda_3^{-1} = 0 \text{ at } Z = 0, H. \tag{24}$$

In the following sections, we specialize the above BVP (24) to a graded neo-Hookean dielectric and discuss the electromechanical behavior including the large deformation, pull-in instability, and the electroactuation. Note that the neo-Hookean model is able to give good agreement with the experiment data at small and moderate strains. However, an apparent discrepancy is found at large strains. The Gent model is usually used to capture the stress-strain relation of an elastomer with nearly full stretched molecular chains [48].

III. GRADED NEO-HOOKEAN DIELECTRICS

Consider a graded neo-Hookean dielectric of which the strain-energy function is

$$W^e(\boldsymbol{F}, \boldsymbol{X}) = \frac{\mu(\boldsymbol{X})}{2}(|\boldsymbol{F}|^2 - 3), \tag{25}$$

where $\mu(\boldsymbol{X})$ is the shear modulus. Note that $\mu(\boldsymbol{X})$ is no longer a constant. It can vary with respect to the cylindrical coordinates R, Θ, and Z.

In this paper, we consider the cylindrical deformations (6) and the related deformations have cylindrical symmetry. To simplify the mathematical derivations, we reduce the generally graded shear modulus $\mu(\boldsymbol{X})$ as a function of only the radius R, i.e., see $\mu(R)$ in Fig. 2; however, the spirit of the effects of graded materials on the nonlinear electromechanical coupling is still kept. By (7) and (8), we have $|\boldsymbol{F}|^2 = \boldsymbol{F} : \boldsymbol{F} = F_{ij}F_{ij} = x^2 + y^2 + \lambda_3^2$, then the strain-energy function (25) can be expressed as

$$W^e = \frac{\mu(R)}{2}(x^2 + y^2 + \lambda_3^2 - 3). \tag{26}$$

By substituting (26) into the BVP (24), the equilibrium equation is

$$(x - y)\frac{\partial}{\partial y}(\mu x - \kappa x^{-1}) + (\mu(x - y) - \kappa(x^{-1} - y^{-1})) = 0, \tag{27}$$

the mechanical boundary conditions are

$$\mu x - \left(\kappa + \frac{\varepsilon\tilde{E}^2\lambda_3^{-2}}{2}\right)x^{-1} = S \quad \text{at } R = B, \tag{28}$$

and

$$\mu\lambda_3 - \left(\kappa - \frac{\varepsilon\tilde{E}^2\lambda_3^{-2}}{2}\right)\lambda_3^{-1} = 0 \quad \text{at } Z = 0, H. \tag{29}$$

The boundary condition (29) indicates that the Lagrange multiplier $\kappa(R)$ has the following relation with respect to the graded shear modulus, namely

$$\kappa(R) = \mu(R)\lambda_3^2 + \frac{\varepsilon\tilde{E}^2\lambda_3^{-2}}{2}. \tag{30}$$

It follows from (28) and (30) that

$$\mu(B)x - (\mu(B)\lambda_3^2 + \varepsilon\tilde{E}^2\lambda_3^{-2})x^{-1} = S \quad \text{at } R = B. \tag{31}$$

Now the BVP only consists of (27) and (31) as well as the equations for kinematics.

A. Solution of the boundary-value problem

Consider the kinematics in the BVP (24). It follows from the constraint of incompressibility, $xy\lambda_3 = 1$, that $rdr = \lambda_3^{-1}RdR$. Integrating both sides, we have

$$r(R) = \sqrt{\lambda_3^{-1}R^2 + C_0}, \tag{32}$$

where C_0 is the constant of integration. By the fact that the center point, $R = 0$, of the circular plate is undeformed during the electromechanical loading process, i.e., $r(0) = 0$, we have $C_0 = 0$. Then (32) is reduced to

$$r(R) = \lambda_3^{-1/2}R. \tag{33}$$

Now the principal stretches in (8) become

$$x = y = \lambda_3^{-1/2}. \tag{34}$$

It follows from $x = y$ in (34) that the equilibrium equation (27) is automatically satisfied. And the only left equation is (31) that is finally represented by

$$\frac{\varepsilon \tilde{E}^2}{\mu(B)} = \left(\lambda_3 - \lambda_3^4\right) - \frac{S}{\mu(B)} \lambda_3^{3/2}. \tag{35}$$

In the algebraic equation (35), if we fix the value of the dead load S, we can consider the applied nominal electric $\tilde{E}$ as an independent variable, while the stretch λ_3 in the thickness direction is the dependent variable. On the other hand, we can fix the applied nominal electric $\tilde{E}$ and consider the dead load S as an independent variable, while the stretch λ_3 is also the dependent variable. To show the above statement, we can write (35) as follows:

$$F(\lambda_3; \tilde{E}, S) = \frac{\varepsilon \tilde{E}^2}{\mu(B)} + \frac{S}{\mu(B)} \lambda_3^{3/2} - \left(\lambda_3 - \lambda_3^4\right) = 0. \tag{36}$$

For a given pair of electromechanical loads $(\tilde{E}, S)$, there exists one or multiple roots of λ_3 in (36). However, only the roots in the range (0, 1] have physical meanings, i.e., the circular dielectric plate shrinks its thickness due to both the dead load in the radial direction and the applied electric field in the thickness direction. Other solutions may be complex roots or negative numbers or positive numbers but greater than 1; and these solutions, of course, have no physical meaning. Therefore, we only consider the roots of λ_3 in the range (0, 1]. Unfortunately, there may exist one or multiple roots or even no roots of λ_3 in the range (0, 1]. In the following, we will discuss the uniqueness of the solution to (36), which is actually the bifurcation analysis in mathematics but is regarded as the analysis of pull-in instability in this paper.

B. Stability analysis

The stability analysis here is actually the analysis of the uniqueness of the solutions to the algebraic equation (36). In the beginning, we consider the case of zero loads $(\tilde{E}, S) = (0, 0)$ in (36), which indicates a root of $\lambda_3 = 1$, and there is no deformation in the circular dielectric plate. As the loads $(\tilde{E}, S)$ increase, the circular dielectric plate is gradually compressed in the thickness direction, i.e., the stretch λ_3 continually decreases from 1.

As the stretch λ_3 decreases to the critical value $\lambda_3^\star$ at the critical loads $(\tilde{E}^\star, S^\star)$, the circular plate cannot sustain the electromechanical loads any more, and then the thickness decreases dramatically if the loads slightly surpass the threshold. The phenomenon is called the occurrence of pull-in instability. The limiting point is denoted by $(\lambda_3^\star; \tilde{E}^\star, S^\star)$, which, of course, satisfy the equilibrium equation (36), such that

$$F(\lambda_3^\star; \tilde{E}^\star, S^\star) = \frac{\varepsilon (\tilde{E}^\star)^2}{\mu(B)} + \frac{S^\star}{\mu(B)} (\lambda_3^\star)^{3/2} - [\lambda_3^\star - (\lambda_3^\star)^4] = 0. \tag{37}$$

By the implicit function theorem, the stretch λ_3 in (36) can be written as a function of $\tilde{E}$, i.e., $\lambda_3 = \bar{\lambda}_3(\tilde{E}; S^\star)$, in the neighborhood of $\bar{E}^\star$ only if the partial derivative $\partial F / \partial \lambda_3$ is nonzero at the limiting point $(\lambda_3^\star; \bar{E}^\star, S^\star)$. On the other hand,

the stretch λ_3 in (36) can be expressed as a function of S, i.e., $\lambda_3 = \hat{\lambda}_3(S; \tilde{E}^\star)$, around $S^\star$ only if $\partial F / \partial \lambda_3$ is nonzero at $(\lambda_3^\star; \tilde{E}^\star, S^\star)$. Therefore, the condition for nonuniqueness solutions at the critical loads $(\bar{E}^\star, S^\star)$ is given by

$$\frac{\partial F}{\partial \lambda_3}(\lambda_3^\star; \tilde{E}^\star, S^\star) = \frac{3}{2} \frac{S^\star}{\mu(B)} (\lambda_3^\star)^{1/2} - [1 - 4(\lambda_3^\star)^3] = 0. \tag{38}$$

In contrast to the equilibrium equation (37), Eq. (38) is the necessary condition for the existence of other solutions bifurcating from the trivial solution. In this paper, Eq. (38) is regarded as the condition for the occurrence of pull-in instability.

There are three parameters $\lambda_3^\star$, $\tilde{E}^\star$, and $S^\star$ in the two algebraic equations (37) and (38). Therefore, either $\tilde{E}^\star$ or $S^\star$ should be given if we want to solve the two algebraic equations. Since both the nominal electric field and the dead load are fixed values during the large deformation, we can track the onset of pull-in instability in two ways. For the first way, we can take the dead load as a properly given value $S^\star$ and gradually increase the magnitude of the nominal electric field $\tilde{E}$ from zero. When $\tilde{E}$ increases to the threshold $\tilde{E}^\star$, pull-in instability occurs and the corresponding value of λ_3 is denoted by $\lambda_3^\star$. The values of $(\lambda_3^\star, \tilde{E}^\star)$ are the solutions to both (37) and (38) for a fixed $S^\star$. In other words, for a properly given $S^\star$, $\tilde{E}^\star$ is the critical electric field and $\lambda_3^\star$ is the critical stretch. For the second way, we can fix $\tilde{E}^\star$ at a properly given value and gradually increase the dead load from zero. When S increases to the threshold $S^\star$, pull-in instability occurs.

IV. RESULTS AND DISCUSSIONS

A. Large deformation and instability of homogeneous dielectrics

For a homogeneous circular dielectric plate (see Fig. 2), the constant shear modulus is given by $\mu(R) = \mu_0$, $0 \leqslant R \leqslant B$. For the stability analysis, the critical stretch $\lambda_3^\star$ at the onset of pull-in instability is obtained from (37) and (38) as $\lambda_3^\star = (\frac{1}{4})^{1/3} = 0.63$, and the critical electric field is $\tilde{E}^\star \sqrt{\varepsilon/\mu_0} = 0.69$. These two critical values are reported by Zhao and Wang in their stability analysis [see the paragraph below Eq. (30) in the work [41]].

In general, we represent the behaviors of the large deformation of a homogeneous circular dielectric plate in Fig. 3. The conditions for the onset of pull-in instability correspond to the peak of each curve.

In Fig. 3(a), we show the change of the stretch λ_3 in the thickness direction with the increase of the dead load S/μ_0 under several electric fields, i.e., $\tilde{E}\sqrt{\varepsilon/\mu_0} = 0, 0.1, 0.2, 0.3$. For the curve corresponding to a zero electric field, the stretch λ_3 decreases from 1 as the dead load S/μ_0 increase from zero, which means that the circular plate expands its in-plane area but shrinks its thickness. Note that the dead load S/μ_0 increases monotonically with the decrease of the thickness (λ_3) and there is no peak in the curve corresponding to a zero electric field. However, the monotonic function only exists for the case of a zero electric field, and nonmonotonic functions occur when the applied electric field is nonzero. To show the effects of the electric field on the large deformation and pull-in instability, we plot three more curves in Fig. 3(a) and find that a larger electric field can compress the circular plate
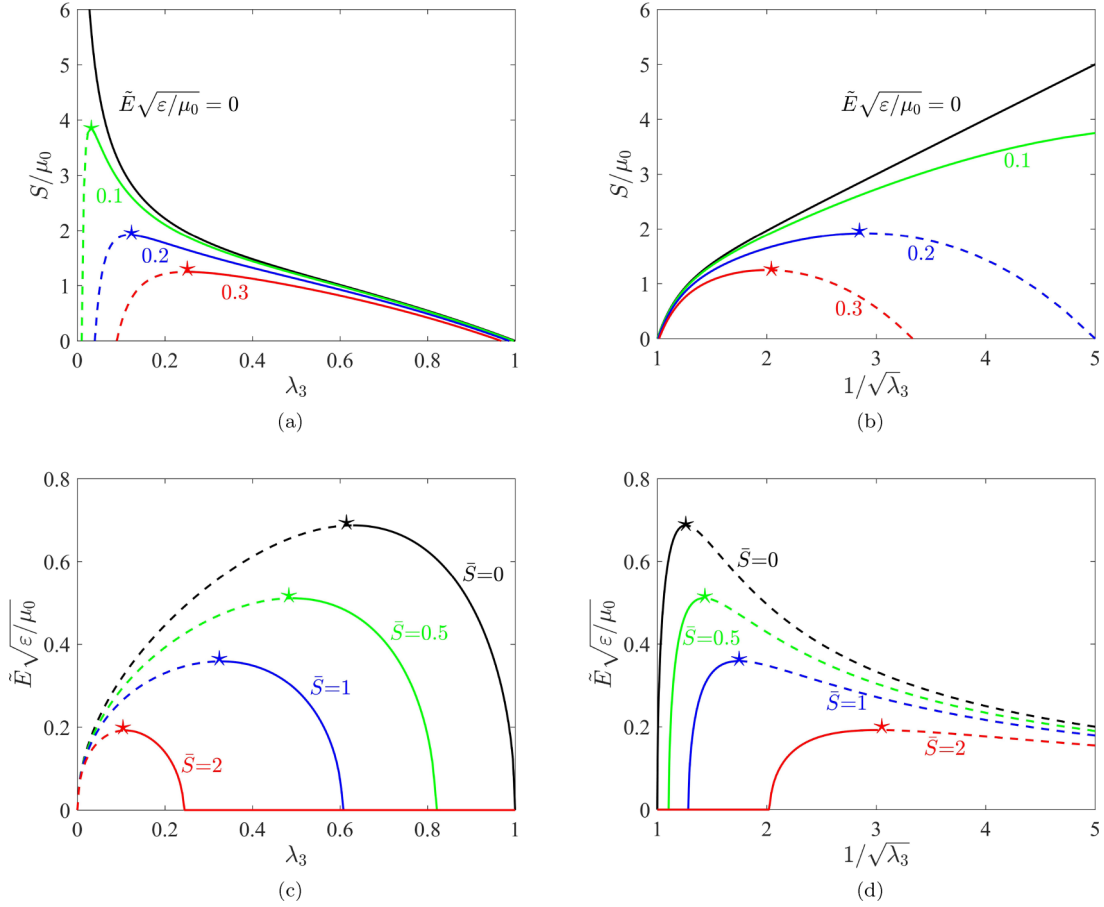
FIG. 3. Large deformation of a homogeneous circular dielectric plate with shear modulus μ_0 subject to electromechanical loads. Under several nominal electric fields $\tilde{E}/\sqrt{\mu_0/\varepsilon} = 0, 0.1, 0.2, 0.3$: (a) stretch λ_3 vs S/μ_0, (b) radial stretch $1/\sqrt{\lambda_3}$ vs S/μ_0. On each curve, the critical point for the onset of pull-in instability is marked by a star ($\star$). Dashed curves represent the unstable equilibrium states. Under several mechanical loads $\bar{S} = S/\mu_0 = 0, 0.5, 1, 2$: (c) stretch λ_3 vs $\tilde{E}/\sqrt{\mu_0/\varepsilon}$, (d) radial stretch $1/\sqrt{\lambda_3}$ vs $\tilde{E}/\sqrt{\mu_0/\varepsilon}$. On each curve, the critical point for the onset of pull-in instability is marked by a star ($\star$). Dashed curves represent the unstable equilibrium states.

more easily. When the circular plate is compressed to the threshold, i.e., the peak denoted by a star "$\star$" on each curve, it cannot sustain the electromechanical loads any more and then pull-in instability occurs. In contrast to the solid curves for the stability parts, the instability parts are plotted by dashed curves. In Fig. 3(b), we plot the variation of the radial stretch $1/\sqrt{\lambda_3}$ with the increase of the dead load S/μ_0 under the same electric field. The large expansion of the radius of the circular plate can make it as an ideal candidate for electric actuators. Also, the onset of pull-in instability is denoted by a star "$\star$" and the instability parts are plotted by dashed curves.

With the increase of the nominal electric field $\tilde{E}\sqrt{\varepsilon/\mu_0}$ under several dead loads, i.e., $S/\mu_0 = 0, 0.5, 1, 2$, we show the change of the stretch λ_3 in Fig. 3(c) and the change of the radial stretch $1/\sqrt{\lambda_3}$ in Fig. 3(d). Subject to purely electric loads, the stretch λ_3 decreases from 1 and the radial stretch $1/\sqrt{\lambda_3}$ increases from 1 when the nominal electric field increases from 0. When $\tilde{E}\sqrt{\varepsilon/\mu_0}$ increases to the threshold, pull-in instability occurs. If one curve corresponds to a larger dead load S/μ_0, the peak in that curve corresponds to a smaller critical nominal electric field, implying that the dead load can assist the occurrence of pull-in instability. When the

electromechanical load surpasses the threshold, the thickness decreases rapidly and the in-plane area increases dramatically until the onset of electric breakdown.

B. Stiffer or softer homogeneous dielectrics

In contrast to homogeneous material I with constant shear modulus μ_0 in Sec. IV A, we consider another homogeneous material (material II) whose shear modulus is given by $\mu(R) = \mu_\gamma$, $0 \leqslant R \leqslant B$, where μ_γ is a constant. Materials I and II are assumed to have the same constant dielectric permittivity ε in this paper.

In order to compare the electromechanical behaviors of *different* homogeneous dielectric elastomers subject to the *same* electromechanical load, we normalize the electromechanical quantities by using the shear modulus μ_0 and the dielectric permittivity ε. Then we can compare the large deformation, pull-in instability, and electroactuation between different dielectric elastomers under the same electromechanical load.

We adopt a scaling in which electric field is measured relative to $\sqrt{\mu_0/\varepsilon}$, and dead load and shear modulus are measured relative to μ_0. This leads to the following dimensionless
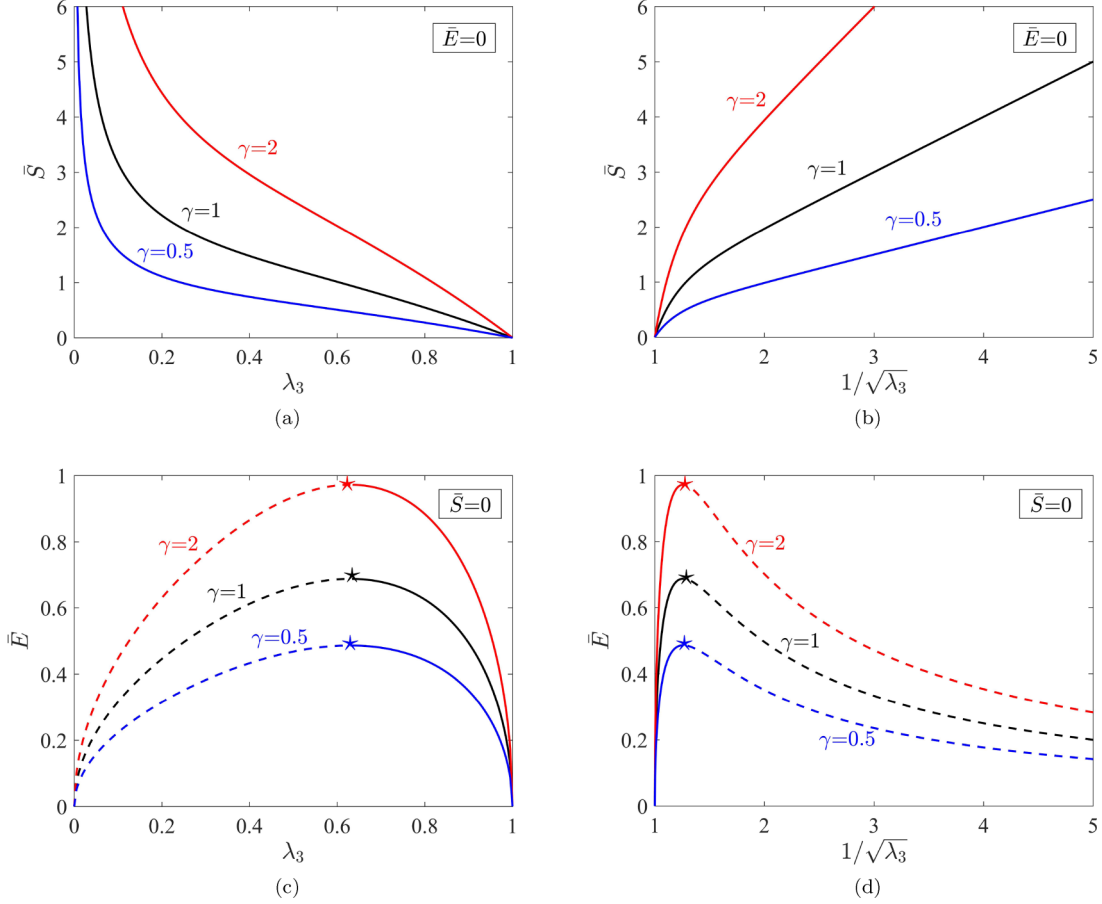
FIG. 4. Large deformation of three different homogeneous circular dielectric plates ($\gamma = 0.5, 1, 2$) subject to the purely mechanical load: (a) stretch λ_3 vs $\bar{S} = S/\mu_0$, (b) radial stretch $1/\sqrt{\lambda_3}$ vs $\bar{S}$, (c) stretch λ_3 vs $\bar{E} = \tilde{E}/\sqrt{\mu_0/\varepsilon}$, (d) radial stretch $1/\sqrt{\lambda_3}$ vs $\bar{E}$. On each curve, the critical point for the onset of pull-in instability is marked by a star ($\star$). Dashed curves represent the unstable equilibrium states.

measures:

$$\left.\begin{array}{ll} \bar{E} = \dfrac{\tilde{E}}{\sqrt{\mu_0/\varepsilon}}, & \bar{S} = \dfrac{S}{\mu_0}, \quad \bar{E}^\star = \dfrac{\tilde{E}^\star}{\sqrt{\mu_0/\varepsilon}}, \\[2mm] \bar{S}^\star = \dfrac{S^\star}{\mu_0}, & \gamma = \dfrac{\mu_\gamma}{\mu_0}. \end{array}\right\} \tag{39}$$

By (39), the equilibrium equation can be rearranged as

$$\bar{E}^2 + \bar{S}\lambda_3^{3/2} - \gamma\left(\lambda_3 - \lambda_3^4\right) = 0, \tag{40}$$

while the stability conditions are

$$\left.\begin{array}{l} (\bar{E}^\star)^2 + \bar{S}^\star(\lambda_3^\star)^{3/2} - \gamma[\lambda_3^\star - (\lambda_3^\star)^4] = 0, \\[2mm] \dfrac{3}{2}\bar{S}^\star(\lambda_3^\star)^{1/2} - \gamma[1 - 4(\lambda_3^\star)^3] = 0. \end{array}\right\} \tag{41}$$

We remark that if the positive constant ratio $\gamma = \mu_\gamma/\mu_0$ is greater (less) than one, material II is stiffer (softer) than material I. In the following, we will discuss the electromechanical behaviors of stiffer or softer homogeneous dielectrics compared to those of material I.

1. Large deformation

It is commonly known that a stiffer elastomer is more difficult to deform compared to a softer one at the same applied

load. We discuss the deformations of three different dielectric films, i.e., $\gamma = 0.5, 1, 2$, subjected to the purely mechanical load at first.

In the absence of an applied electric field ($\bar{E} = 0$), the stretch λ_3 in the thickness direction is plotted in Fig. 4(a) while the radial stretch $1/\sqrt{\lambda_3}$ is plotted in Fig. 4(b) for different dielectric films. At the same λ_3 for different dielectric films in Fig. 4(a), a stiffer film ($\gamma = 2$) corresponds to a larger applied load $\bar{S}$ while a softer film ($\gamma = 0.5$) corresponds to a smaller $\bar{S}$ compared to that of the reference film ($\gamma = 1$). On the other hand, at the same $\bar{S}$ for different dielectric films in Fig. 4(a), a stiffer film ($\gamma = 2$) corresponds to a larger stretch λ_3 while a softer film ($\gamma = 0.5$) corresponds to a smaller stretch λ_3 compared to that of the reference film ($\gamma = 1$). Opposite effects can be seen in Fig. 4(b). For example, at the same $\bar{S}$ for different dielectric films in Fig. 4(b), a stiffer film ($\gamma = 2$) corresponds to a smaller radial stretch $1/\sqrt{\lambda_3}$ and a softer film ($\gamma = 0.5$) corresponds to a larger radial stretch $1/\sqrt{\lambda_3}$ compared to that of the reference film ($\gamma = 1$). In short, Figs. 4(a) and 4(b) demonstrate the fact that a stiffer film is able to sustain a larger mechanical load, and vice versa.

It is obvious in Figs. 4(a) and 4(b) that the variation of each curve is monotonic and there is no peak due to the property of stiffening in neo-Hookean solids subjected to the purely mechanical load. However, the applied electric field
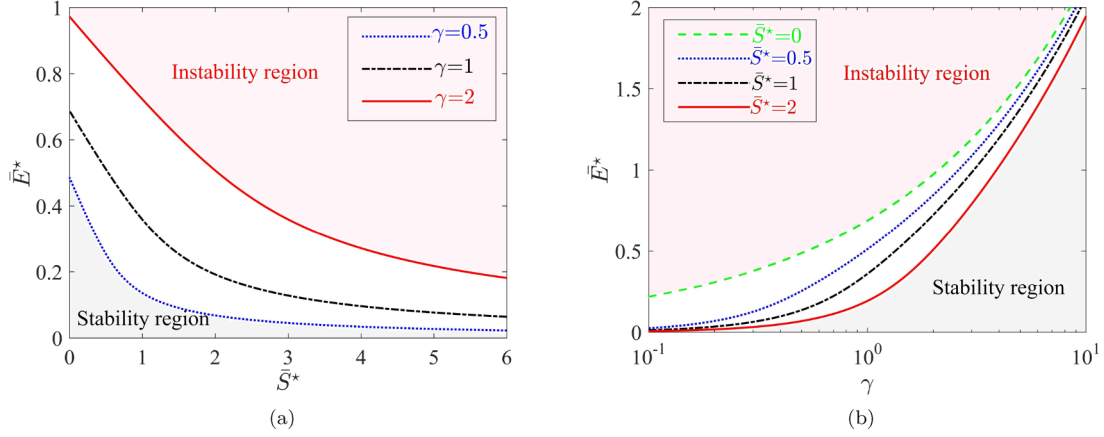
FIG. 5. The critical nominal electric field $\bar{E}^{\star} = \tilde{E}^{\star}/\sqrt{\mu_0/\varepsilon}$ for the onset of pull-in instability. (a) Critical mechanical load $\bar{S}^{\star} = S^{\star}/\mu_0$ vs $\bar{E}^{\star}$ for three different homogeneous circular dielectric plates ($\gamma = 0.5, 1, 2$). (b) Normalized shear modulus $\gamma = \mu/\mu_0$ vs $\bar{E}^{\star}$ under several dead loads ($\bar{S}^{\star} = 0, 0.5, 1, 2$).

can make each curve vary nonmonotonically. To directly show the effects of the electric field on the large deformation, we exclude the dead load ($\bar{S} = 0$) in Figs. 4(c) and 4(d). At the same stretch λ_3 or the same radial stretch $1/\sqrt{\lambda_3}$ for different dielectric films, a stiffer film ($\gamma = 2$) corresponds to a larger nominal electric field $\bar{E}$ and a softer film ($\gamma = 0.5$) corresponds to a smaller nominal electric field $\bar{E}$ compared to that of the reference film ($\gamma = 1$). Moreover, a stiffer film can sustain a higher critical nominal electric field (the "$\star$" marked on each curve), which indicates that pull-in instability is not easy to occur in stiffer films compared to softer films. After the deformation surpasses the threshold, the film cannot sustain the electric load any more and then the equilibrium state is unstable. We represent the unstable states by using dashed curves.

2. Pull-in instability

In this section, we investigate the critical nominal electric field ($\tilde{E}^{\star}$) for the occurrence of pull-in instability. For a homogeneous circular dielectric plate with the normalized shear modulus γ, one can get the critical stretch $\lambda_3^{\star}$ at a given dead load $\bar{S}^{\star} > 0$ by using $(41)_2$. Then the substitution of the obtained $\lambda_3^{\star}$ into $(41)_1$ gives the critical nominal electric field $\bar{E}^{\star}$.

We plot the stability and instability regions of different homogeneous dielectric elastomers on the $\bar{S}^{\star}$–$\bar{E}^{\star}$ plane in Fig. 5(a). The stability and instability regions of each material ($\gamma = 0.5, 1, 2$) are separated by a smooth curve, which is the solution $\bar{E}^{\star}$ of (41) for an applied dead load $\bar{S}^{\star}$. There is no pull-in instability and the circular dielectric plate is stable if the applied electric field is less than the threshold $\bar{E}^{\star}$. On the contrary, when the electromechanical load is in the instability region, pull-in instability occurs and then the thinning of the circular plate is rapid, and finally, electric breakdown will break the circular plate at a relatively high true electric field. The discussion of electric breakdown is omitted here.

In Fig. 5(a), a stiffer film ($\gamma = 2$) corresponds to a larger stability region and a softer film ($\gamma = 0.5$) corresponds to a smaller stability region compared to that of the reference film ($\gamma = 1$). In other words, a stiffer film is able to sustain a

larger electromechanical load and is more difficult to become unstable, and vice versa. As the dead load $\bar{S}^{\star}$ increases, the critical nominal electric field $\bar{E}^{\star}$ decreases monotonically, which shows that pull-in instability can occur at a relatively low $\bar{E}^{\star}$ with the assistance of the dead load. In Fig. 5(b), we plot the critical nominal electric field $\bar{E}^{\star}$ with the variation of the normalized shear modulus γ, which clearly shows that $\bar{E}^{\star}$ increases monotonically with the increase of γ.

Though a stiffer film has a higher critical nominal electric field, its corresponding deformation is smaller than that of a softer film. In the following, we will use different homogeneous dielectric elastomers to show the maximum deformation at which the critical electromechanical load ($\bar{S}^{\star}, \bar{E}^{\star}$) makes pull-in instability occur.

3. Electroactuation

In this section, we focus on the critical stretch and the maximum electroactuation of a circular dielectric plate subjected to the critical nominal electric field ($\bar{E}^{\star}$) and the corresponding dead load ($\bar{S}^{\star}$).

As stated in Sec. IV B 2, one can get the critical stretch $\lambda_3^{\star}$ in the thickness direction at a given pair of loads ($\bar{E}^{\star}, \bar{S}^{\star}$) by using $(41)_2$, such that

$$\tfrac{3}{2}\bar{S}^{\star}(\lambda_3^{\star})^{1/2} = \gamma[1 - 4(\lambda_3^{\star})^3]. \tag{42}$$

In contrast to $\lambda_3^{\star}$, the pre-stretch in the thickness direction is denoted by λ_3^p, which corresponds to the deformation caused by only the dead load $\bar{S}^{\star}$. Explicitly, λ_3^p is the solution of $(41)_1$ at $\bar{E}^{\star} = 0$, namely

$$\bar{S}^{\star}(\lambda_3^p)^{1/2} = \gamma\left[1 - (\lambda_3^p)^3\right]. \tag{43}$$

By (42) and (43), we define the maximum actuation stretch in the thickness direction as $\lambda_3^{\star}/\lambda_3^p$; meanwhile, the corresponding maximum actuation stretch in the radial direction is equal to $\sqrt{\lambda_3^p}/\sqrt{\lambda_3^{\star}}$. At first, we discuss four limiting cases of (42) and (43) analytically.

(1.) At a zero dead load $\bar{S}^{\star} = 0$, the critical stretch $\lambda_3^{\star}$ in (42) is equal to 0.63 while the pre-stretch λ_3^p in (43) is 1 for any dielectric elastomer ($\gamma > 0$). Thus, the maximum actuation stretch in the thickness direction is $\lambda_3^{\star}/\lambda_3^p = 0.63$ while the
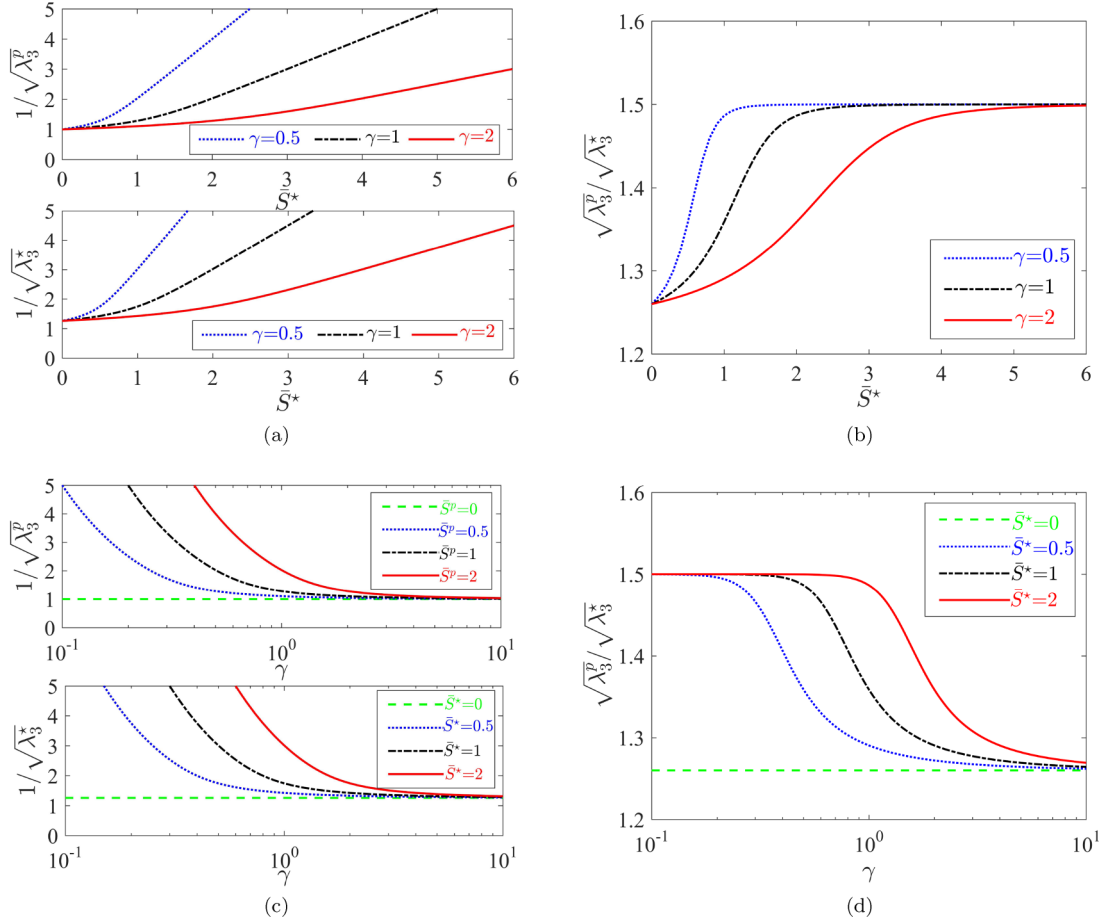
FIG. 6. Maximum electroactuation of different homogeneous circular dielectric plates subject to electromechanical loads. (a) Dead load $\bar{S}^\star = S^\star/\mu_0$ vs pre-stretch $1/\sqrt{\lambda_3^p}$ and critical stretch $1/\sqrt{\lambda_3^\star}$ in the radial direction. For any homogeneous circular dielectric plate, $1/\sqrt{\lambda_3^p} \to 1$ and $1/\sqrt{\lambda_3^\star} \to 1.26$ as $\bar{S}^\star \to 0$. (b) Dead load $\bar{S}^\star$ vs maximum electrostretch $\sqrt{\lambda_3^p}/\sqrt{\lambda_3^\star}$ in the radial direction. As $\bar{S}^\star$ increases from 0 to ∞, $\sqrt{\lambda_3^p}/\sqrt{\lambda_3^\star}$ increases from 1.26 to 1.5. (c) Normalized shear modulus γ vs pre-stretch $1/\sqrt{\lambda_3^p}$ and critical stretch $1/\sqrt{\lambda_3^\star}$ in the radial direction. For $\bar{S}^\star \neq 0$, $1/\sqrt{\lambda_3^p} \to 1$, and $1/\sqrt{\lambda_3^\star} \to 1.26$ as $\gamma \to \infty$. (d) Normalized shear modulus γ vs maximum electrostretch $\sqrt{\lambda_3^p}/\sqrt{\lambda_3^\star}$ in the radial direction.

maximum actuation stretch in the radial direction is equal to $\sqrt{\lambda_3^p}/\sqrt{\lambda_3^\star} = 1.26$.

(2.) As the dead load $\bar{S}^\star$ approaches ∞, both $\lambda_3^\star$ and λ_3^p are approximately proportional to $(\bar{S}^\star)^{-2}$, i.e., $\lambda_3^\star, \lambda_3^p \to 0$ and $1/\sqrt{\lambda_3^\star}, 1/\sqrt{\lambda_3^p} \to \infty$ as $\bar{S}^\star \to \infty$. By dropping $\bar{S}^\star$ in (42) and (43), we have the maximum actuation stretch in the radial direction in the form $\sqrt{\lambda_3^p}/\sqrt{\lambda_3^\star} = \frac{3}{2}\frac{1-(\lambda_3^p)^3}{1-4(\lambda_3^\star)^3}$. Then we have $\sqrt{\lambda_3^p}/\sqrt{\lambda_3^\star} \to \frac{3}{2}$ as $\bar{S}^\star \to \infty$.

(3.) As the normalized shear modulus γ approaches zero for $\bar{S}^\star \neq 0$, both $\lambda_3^\star$ and λ_3^p are proportional to γ^2, i.e., $\lambda_3^\star, \lambda_3^p \to 0$ and $1/\sqrt{\lambda_3^\star}, 1/\sqrt{\lambda_3^p} \to \infty$ as $\gamma \to 0$. Then we have $\sqrt{\lambda_3^p}/\sqrt{\lambda_3^\star} \to \frac{3}{2}$ as $\gamma \to 0$.

(4.) As the normalized shear modulus $\gamma \to \infty$ for $\bar{S}^\star \neq 0$, Eq. (42) implies $[1 - 4(\lambda_3^\star)^3] \to 0$ and then $\lambda_3^\star \to 0.63$. Also, Eq. (43) implies $[1 - (\lambda_3^p)^3] \to 0$ and then $\lambda_3^p \to 1$. Therefore, we have $\sqrt{\lambda_3^p}/\sqrt{\lambda_3^\star} \to 1.26$ as $\gamma \to \infty$.

In addition to the four limiting cases, we plot the pre-stretch, the critical stretch, and the maximum electroactuation stretch in the radial direction numerically. The analytical results of the four limiting cases can also be found in the numerical plots in Fig. 6.

In Fig. 6(a), we plot the pre-stretch $1/\sqrt{\lambda_3^p}$ and the critical stretch $1/\sqrt{\lambda_3^\star}$ vs the dead load $\bar{S}^\star$ curves for three different dielectrics. At a given dead load $\bar{S}^\star > 0$, a stiffer film ($\gamma = 2$) corresponds to both smaller $1/\sqrt{\lambda_3^p}$ and $1/\sqrt{\lambda_3^\star}$ compared to that of the reference film ($\gamma = 1$), and vice versa. As $\bar{S}^\star \to 0$, $1/\sqrt{\lambda_3^p} \to 1$, and $1/\sqrt{\lambda_3^\star} \to 1.26$, which have been shown analytically in the first limiting case. In short, Fig. 6(a) indicates that a softer film corresponds to a larger pre-stretch and a larger critical stretch in the radial direction at a given dead load, and vice versa. This behavior becomes more obvious when the dead load becomes larger. Does it mean that a softer dielectric elastomer has a larger electroactuation? To answer this question, we have to investigate the electroactuation.

In Fig. 6(b), we plot the variation of the maximum electroactuation stretch in the radial direction, $\sqrt{\lambda_3^p}/\sqrt{\lambda_3^{\star}}$, with the increase of the dead load. Without the dead load, different dielectric films have the same maximum actuation stretch, i.e., $\sqrt{\lambda_3^p}/\sqrt{\lambda_3^{\star}} = 1.26$ at $\bar{S}^{\star} = 0$. By increasing the dead load, the maximum electroactuation stretch increases monotonically, and the softest dielectric ($\gamma = 0.5$) has the fastest increase. Eventually, the maximum actuation stretch $\sqrt{\lambda_3^p}/\sqrt{\lambda_3^{\star}}$ of all the three dielectrics approaches 1.5 as $\bar{S}^{\star} \to \infty$. In short, for any circular dielectric plate, $\sqrt{\lambda_3^p}/\sqrt{\lambda_3^{\star}} \to 1.26$ as $\bar{S}^{\star} \to 0$ and $\sqrt{\lambda_3^p}/\sqrt{\lambda_3^{\star}} \to 1.5$ as $\bar{S}^{\star} \to \infty$.

Figure 6(c) presents the pre-stretch $1/\sqrt{\lambda_3^p}$ and the critical stretch $1/\sqrt{\lambda_3^{\star}}$ vs the normalized shear modulus γ under several dead loads. Figure 6(d) plots the maximum electroactuation stretch $\sqrt{\lambda_3^p}/\sqrt{\lambda_3^{\star}}$ in the radial direction vs γ. We omit the detailed discussions here since they are similar to that of Figs. 6(a) and 6(b).

Figures 6(a)–6(d) provide a useful guideline for the design of a circular dielectric plate actuator. Its maximum electroactuation stretch in the radial direction can vary from 1.26 to 1.5 by changing the modulus or the pre-loads.

C. Graded dielectrics

Recalling the equilibrium equation (36) and the conditions (37) and (38) for the onset of pull-in instability, we only have to use the shear modulus $\mu(B)$ on the outer surface. In other words, the magnitude of the shear modulus within the circular dielectric plate is unimportant for the nonlinear behavior of the electromechanical coupling.

As shown in Fig. 2, the shear modulus $\mu(R)$ can be either an increasing function $\mu_1(R)$ or a deceasing function $\mu_2(R)$ with respect to the radius R. The variation of the modulus depends on the manufacturing process of a graded circular dielectric plate. In this paper, we show it theoretically that the electromechanical coupling only depends on the modulus at $R = B$. In other words, if two graded dielectrics $\mu_1(R)$ and $\mu_2(R)$ have the same modulus as that of a homogeneous dielectric μ_0 at $R = B$, i.e., $\mu_1(B) = \mu_2(B) = \mu_0$, subjected to the same electromechanical loads, these three *different* circular dielectric plates can present the *same* behavior of large deformation and electromechanical instability.

To understand and harness the unique property of a graded circular dielectric plate proposed in this paper, we compare the large deformation, pull-in instability, and electroactuator in several homogeneous circular dielectric plates with different moduli. If we want to take advantage of the large deformation and actuation existing in the soft homogeneous circular dielectric plate, for example, the conventional way is to change the whole circular plate from a stiff dielectric to a soft dielectric. However, by utilizing the unique property of a graded circular dielectric plate, we only have make the outer region of a circular dielectric plate as soft as needed, which can present exactly the same electromechanical behavior as that of a soft homogeneous circular dielectric plate. On the other hand, if we want to utilize the relatively high critical nominal electric field existing in the stiff homogeneous circular dielectric plate, we only have to make the outer region of a circular dielectric plate as stiff as wanted, which can present exactly the same electromechanical behavior as that of a stiff homogeneous one.

V. CONCLUDING REMARKS

This paper is motivated by the long-standing interest in the fundamental understanding of the nonlinear coupling behaviors in soft dielectrics. We study the effects of the material inhomogeneity on the large deformation, pull-in instability, and electroactuation in graded soft dielectrics. By using an assumed homogeneous thinning in a graded neo-Hookean dielectric, our theoretical results show that the large deformation and the conditions for the occurrence of pull-in instability *only* depend on the shear modulus of the circular plate at its outer radius. The results of homogeneous soft dielectrics obtained in this paper agree with the electromechanical behaviors of homogeneous dielectric plates [18,41].

Our simple theoretical model also shows that the maximum radial electroactuation can vary from 1.26 to 1.5 by changing either the dead load or the modulus. It implies that an optimized electroactuation can be achieved by partly changing the modulus of the circular plate. The results could be useful for the design and the optimization of soft graded dielectric actuators.

We remark here that the failure mode of electric breakdown is excluded, and the competition between pull-in instability and electric breakdown is not presented in this paper. Yet one future research direction can be the investigation of electric breakdown in graded dielectrics. Another research direction could be the investigation of nonlinear electromechanical coupling in graded soft materials of different geometries, including the graded cylinders and spheres. It is hoped that the analysis of the electromechanical coupling in graded dielectrics will help in the design of advanced dielectric devices capable of high critical electric field and giant electroactuation.

[1] R. Pelrine, R. Kornbluh, Q. Pei, and J. Joseph, Science **287**, 836 (2000).

[2] R. Pelrine, R. Kornbluh, J. Joseph, R. Heydt, Q. Pei, and S. Chiba, Mater. Sci. Eng. C **11**, 89 (2000).

[3] R. Shankar, T. K. Ghosh, and R. J. Spontak, Soft Matter **3**, 1116 (2007).

[4] G. Kofod, W. Wirges, M. Paajanen, and S. Bauer, Appl. Phys. Lett. **90**, 081916 (2007).

[5] C. Keplinger, M. Kaltenbrunner, N. Arnold, and S. Bauer, Proc. Natl. Acad. Sci. **107**, 4505 (2010).

[6] D. Rus and M. T. Tolley, Nature (London) **521**, 467 (2015).

[7] S. Shian, K. Bertoldi, and D. R. Clarke, Adv. Mater. **27**, 6814 (2015).

[8] J. A. Rogers, T. Someya, and Y. Huang, Science **327**, 1603 (2010).

[9] N. Lu and D.-H. Kim, Soft Rob. **1**, 53 (2014).

[10] S. J. A. Koh, X. Zhao, and Z. Suo, Appl. Phys. Lett. **94**, 262902 (2009).

[11] S. J. A. Koh, C. Keplinger, T. Li, S. Bauer, and Z. Suo, IEEE/ASME Trans. Mechatron. **16**, 33 (2011).

[12] J. Huang, S. Shian, Z. Suo, and D. R. Clarke, Adv. Funct. Mater. **23**, 5056 (2013).

[13] S. Bauer, S. Bauer-Gogonea, I. Graz, M. Kaltenbrunner, C. Keplinger, and R. Schwödiauer, Adv. Mater. **26**, 149 (2014).

[14] Q. Deng, M. Kammoun, A. Erturk, and P. Sharma, Int. J. Solids Struct. **51**, 3218 (2014).

[15] S. Yang, X. Zhao, and P. Sharma, Soft Matter **13**, 4552 (2017).

[16] K. Stark and C. Garton, Nature (London) **176**, 1225 (1955).

[17] J.-S. Plante and S. Dubowsky, Int. J. Solids Struct. **43**, 7727 (2006).

[18] X. Zhao and Z. Suo, Appl. Phys. Lett. **91**, 061921 (2007).

[19] X. Zhao and Z. Suo, Appl. Phys. Lett. **95**, 031904 (2009).

[20] X. Zhao and Z. Suo, Phys. Rev. Lett. **104**, 178302 (2010).

[21] B.-X. Xu, R. Mueller, M. Klassen, and D. Gross, Appl. Phys. Lett. **97**, 162908 (2010).

[22] B. Li, J. Zhou, and H. Chen, Appl. Phys. Lett. **99**, 244101 (2011).

[23] J. Huang, T. Li, C. Chiang Foo, J. Zhu, D. R. Clarke, and Z. Suo, Appl. Phys. Lett. **100**, 041911 (2012).

[24] L. Jiang, A. Betts, D. Kennedy, and S. Jerrams, J. Phys. D: Appl. Phys. **49**, 265401 (2016).

[25] B. Tavakol, M. Bozlar, C. Punckt, G. Froehlicher, H. A. Stone, I. A. Aksay, and D. P. Holmes, Soft Matter **10**, 4789 (2014).

[26] H. Bense, M. Trejo, E. Reyssat, J. Bico, and B. Roman, Soft Matter **13**, 2876 (2017).

[27] S. Yang, X. Zhao, and P. Sharma, J. Appl. Mech. Trans. ASME **84**, 031008 (2017).

[28] A. Dorfmann and R. W. Ogden, Int. J. Eng. Sci. **48**, 1 (2010).

[29] H. Godaba, Z.-Q. Zhang, U. Gupta, C. C. Foo, and J. Zhu, Soft Matter **13**, 2942 (2017).

[30] Q. Wang and X. Zhao, Phys. Rev. E **88**, 042403 (2013).

[31] G. Zurlo, M. Destrade, D. DeTommasi, and G. Puglisi, Phys. Rev. Lett. **118**, 078001 (2017).

[32] Q. Wang, Z. Suo, and X. Zhao, Nat. Commun. **3**, 1157 (2012).

[33] M. Pharr, J.-Y. Sun, and Z. Suo, J. Appl. Phys. **111**, 104114 (2012).

[34] L. Zhang, Q. Wang, and X. Zhao, Appl. Phys. Lett. **99**, 171906 (2011).

[35] J. Huang, S. Shian, R. M. Diebold, Z. Suo, and D. R. Clarke, Appl. Phys. Lett. **101**, 122905 (2012).

[36] P. Brochu and Q. Pei, Macromol. Rapid Commun. **31**, 10 (2010).

[37] Q. Wang, D. Robinson, and X. Zhao, Appl. Phys. Lett. **104**, 231605 (2014).

[38] C. Keplinger, T. Li, R. Baumgartner, Z. Suo, and S. Bauer, Soft Matter **8**, 285 (2012).

[39] T. Li, C. Keplinger, R. Baumgartner, S. Bauer, W. Yang, and Z. Suo, J. Mech. Phys. Solids **61**, 611 (2013).

[40] A. J. Crosby, Soft Matter **6**, 5660 (2010).

[41] X. Zhao and Q. Wang, Appl. Phys. Rev. **1**, 021304 (2014).

[42] N. Hu and R. Burgueño, Smart Mater. Struct. **24**, 063001 (2015).

[43] G. Kofod, J. Phys. D: Appl. Phys. **41**, 215405 (2008).

[44] S. M. Ha, W. Yuan, Q. Pei, R. Pelrine, and S. Stanford, Adv. Mater. **18**, 887 (2006).

[45] X. Niu, H. Stoyanov, W. Hu, R. Leo, P. Brochu, and Q. Pei, J. Polym. Sci., Part B: Polym. Phys. **51**, 197 (2013).

[46] S. Yang and Y.-c. Chen, Proc. R. Soc. A **473**, 20160882 (2017).

[47] Z. Suo, X. Zhao, and W. H. Greene, J. Mech. Phys. Solids **56**, 467 (2008).

[48] A. Gent, Rubber Chem. Technol. **69**, 59 (1996).

[49] M. Wissler and E. Mazza, Sens. Actuators, A **138**, 384 (2007).

[50] X. Zhao and Z. Suo, J. Appl. Phys. **104**, 123530 (2008).